A Novel Deposit/Spin Waveguide Interconnection (DSWI) for Semiconductor Integrated Optics

KAZUHITO FURUYA, MEMBER, IEEE, BARRY I. MILLER, LARRY A. COLDREN, FELLOW, IEEE, AND RICHARD E. HOWARD, MEMBER, IEEE

Abstract—**We propose an efficient and simple optical interconnection between active semiconductor components by deposition and spin coating. Details of the waveguide design, the fabrication technique, and a promising material combination are given. Experimental results with an integrated laser-polyimide/SiO_x ($x \sim 2$) waveguide combination demonstrate low-threshold (2.0 kA/cm^2) laser operation and a low-loss waveguide interconnection (81 percent coupling efficiency) on a GaInAsP/InP chip.**

I. Introduction

OPTICAL interconnection is a key to realizing practical monolithic integrated optics. In particular, semiconductor integrated optical circuits require low-loss passive waveguides to interconnect active components arranged on a chip. In addition, the fabrication technique must be simple such as the conventional "metallization" process in electronic integrated circuits.

Two methodologies for integrating passive interconnecting waveguides in a semiconductor crystal have been proposed. The first utilizes semiconductor material for fabricating passive waveguides in laser crystals [1], [2] such as AlGaAs and GaInAsP/InP. This technique has been used to integrate active and passive optical circuit components such as lasers [3]-[6], [8]-[16], waveguides [5], [9], [12]-[14], distributed Bragg reflectors [4], [8], [11], [16], modulators [3], [6], amplifiers [6], [10], and detectors [10], [15]. However, they are complex and require precise control in a crystal growth or additional regrowth of the crystal after patterning.

The second methodology involves the fabrication of dielectric waveguides for the interconnection, in which a low-index dielectric layer is isolated from a high-index crystal substrate by a metal cladding [17] or an SiO_2 layer on a silicon wafer substrate [18]-[21]. Although the latter technique (silicon substrate) has been used to integrate certain optical components, such as filters [18] and detectors [18]-[20], with dielectric waveguides that have lower absorption loss [19]-[21] than semiconductor waveguides, their reliance on silicon technology and thermally grown SiO_2 buffer layers makes them inapplicable for monolithic integration on laser crystals. Neither of these two methodologies described above addresses the problem of fabricating a monolithically integrated optical circuit which includes dielectric waveguides.

A number of basic schemes of coupling between active and passive waveguides and components have been proposed, for example, phase coupling [9], butt coupling [12], mode-profile-matched butt coupling [7], evanescent coupling [14], [15], and taper coupling [4], [22]. The mode-profile-matched butt coupling is a particularly promising scheme with respect to high efficiency and no restriction on device length by a coupling length.

Concerning basic fabrication techniques for monolithic integration, etching techniques for a facet formation on an active component have been developed on AlGaAs [15] and InGaAsP/InP [23]-[27]. Air gap coupling between integrated InGaAsP/InP devices with etched facets has demonstrated laser/detector [24], [28] and laser/laser [28] combinations. Improvements in the quality and reproducibility of the exposed facet have been achieved by using an orientational stop-etching property in InGaAsP/InP wet chemical etching [29].

Here we propose a novel deposit/spin waveguide interconnection (DSWI) technique [30] to provide light transmission between etched facets of active components through a dielectric waveguide. Facets on active components and substrates for the interconnecting dielectric waveguides are exposed by an orientational and material selective etching technique [29]. These waveguides are formed by thin-film deposition and polymer spin coating with relatively large tolerances and with stable dielectric materials. The basic coupling scheme between the active and the passive waveguides is a butt joint with a matched mode profile. For these reasons, DSWI is different from any previously proposed interconnection method.

In this paper, we present the DSWI technique, and discuss the design, material, and fabrication techniques. To demonstrate a promising material combination, we present a laser-polyimide/SiO_x ($x \sim 2$) waveguide integrated on a GaInAsP/InP chip. We attained low-threshold and high-coupling operation using the newly developed etched facets butt-jointed with the interconnecting waveguide.

II. Outline of DSWI Technique

The processes for DSWI are outlined in Fig. 1(a). The first step is the creation of vertical facets at the ends of active components and flat horizontal surfaces between them. In order to avoid a scattering loss at the facet or the passive waveguide due to a tilt or roughness, the exposed vertical and horizontal surfaces must be sufficiently smooth and perpendicular to

Manuscript received March 2, 1982; revised May 19, 1982.

K. Furuya is with Bell Laboratories, Holmdel, NJ 07733, on leave from the Tokyo Institute of Technology, Tokyo 152, Japan.

B. I. Miller, L. A. Coldren, and R. E. Howard are with Bell Laboratories, Holmdel, NJ 07733.

0018-9480/82/1000-1771$00.75 © 1982 IEEE

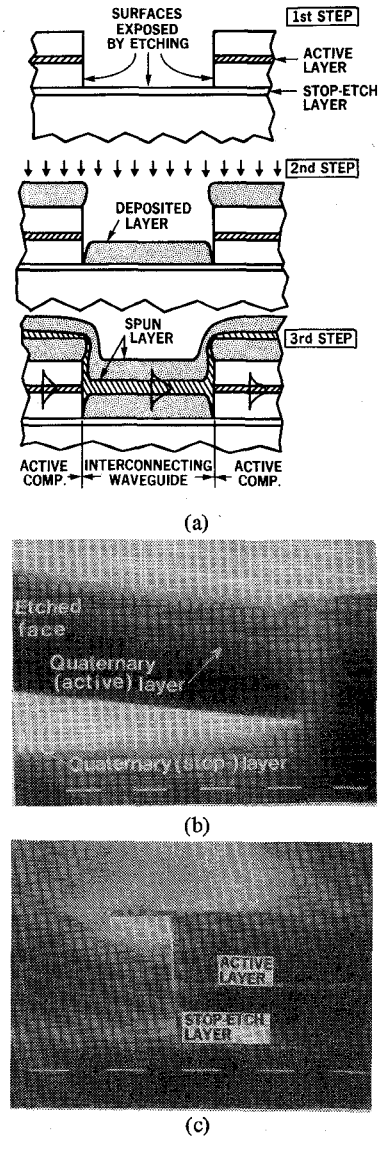

Fig. 1. DSWI technique: (a) fabrication processes. (b) and (c), a result of the orientational and material selective etching: marker is 1 μm.

each other. For this purpose, we can expose crystallographic surfaces by including a stop-etch layer in the heterostructure as shown in Fig. 1(a) and using an orientational and material selective etching technique. Our technique [29], as shown in Fig. 1(b) and (c), exposes smooth and flat crystallographic planes. Coating the facet with dielectric films controls the facet reflectivity.

The second step is the deposition of a dielectric material to form the lower cladding layer of the interconnecting waveguide. The thickness of this cladding layer must be sufficient to avoid radiation loss due to the higher index stubstrate as given theoretically in [31]. Vacuum deposition provides a sharp edge, as shown in Fig. 1(a). Room temperature deposition at a slow rate enables accurate control of the thickness of the deposited layer and a low thermal stress.

The next step is a spin coating of a dielectric material to form the core of the waveguide. As an advantage of using a liquid coating, slight gaps between the etched facets and the ends of the deposited layers are filled up to result in a smooth connection. Photolithographic patterning of the spun layer forms a two-dimensional waveguide, such as a rib waveguide [32], and the desired optical interconnection paths. A spin coating or the deposition of another dielectric material forms the upper cladding layer of the waveguide and simultaneously passivates the surface of the chip.

III. Materials for DSWI

A. Cladding Layer

A stable and easy-to-vacuum deposit film with a low refractive index is desirable for the cladding layer of the passive waveguide. We chose a silicon dioxide film for this purpose.

The silicon dioxide film was formed by thermal evaporation of silicon monoxide in 2×10^{-4} mbar of oxygen at a rate of 5 Å/s onto a room temperature substrate. The deposited material is generally SiO_x, with the value of x, and therefore the refractive index, controlled by the oxygen pressure and the deposition rate [33]. In our case, the refractive index of the deposited film was measured to be 1.55 by ellipsometry at a wavelength of 0.6328 μm. The stoichiometry of the deposited material was not studied in detail. However, by comparing the refractive index to those of SiO and SiO_2, 1.996 and 1.46, respectively, the deposited material was closer to SiO_2 rather than to SiO.

In order to prevent undesired deposits on vertical facets, the deposition must be done at normal incidence. However, even in this case, a certain amount of "overhang" on the top layer and a V-shaped "gap" beside the vertical facet were formed, as depicted in Fig. 1(a); a typical gap width was 0.3 μm. In the case of E-beam evaporation of silicon dioxide, larger "overhangs" and wider "gaps" resulted.

A silicon dioxide film of 2 μm thickness deposited as mentioned above adhered to the InGaAsP surface well and did not peel off, even with heating up to 500°C.

B. Core Layer

For the core layer of the passive waveguide, a stable and easily spin-coated film with a high refractive index is desirable. For this purpose, we examined polyimide [34] which is sufficiently stable to be used in electronic integrated circuits as a passivating material [35].

Spectral transmission characteristics were measured as follows: a polyimide film of 120 μm thickness was coated on a glass slide, cured at 200°C in air for 2 h, and measured with a Cary recording spectrophotometer. As shown in Fig. 2(a), the polyimide is transparent for infrared wavelengths longer than 0.85 μm.

The spectral refractive index was measured using a similar film, on a Si substrate in this case, by taking reflectance data from the Cary. The thickness of the spun polyimide film was measured by a stylus instrument to be 1.9 ± 0.1 μm. From the wavelengths of the maximum and the minimum reflection, the refractive index of the film was calculated [36] as shown in Fig. 2(b).

As can be seen in Fig. 2(b), the polyimide has refractive index of 1.72 in a wavelength region from 0.85 to 1.8 μm, a higher index than that of conventional photoresist and electron resist materials [19]. The refractive index increases for wavelengths less than 0.85 μm, corresponding to the increase in the loss as shown in Fig. 2(a).

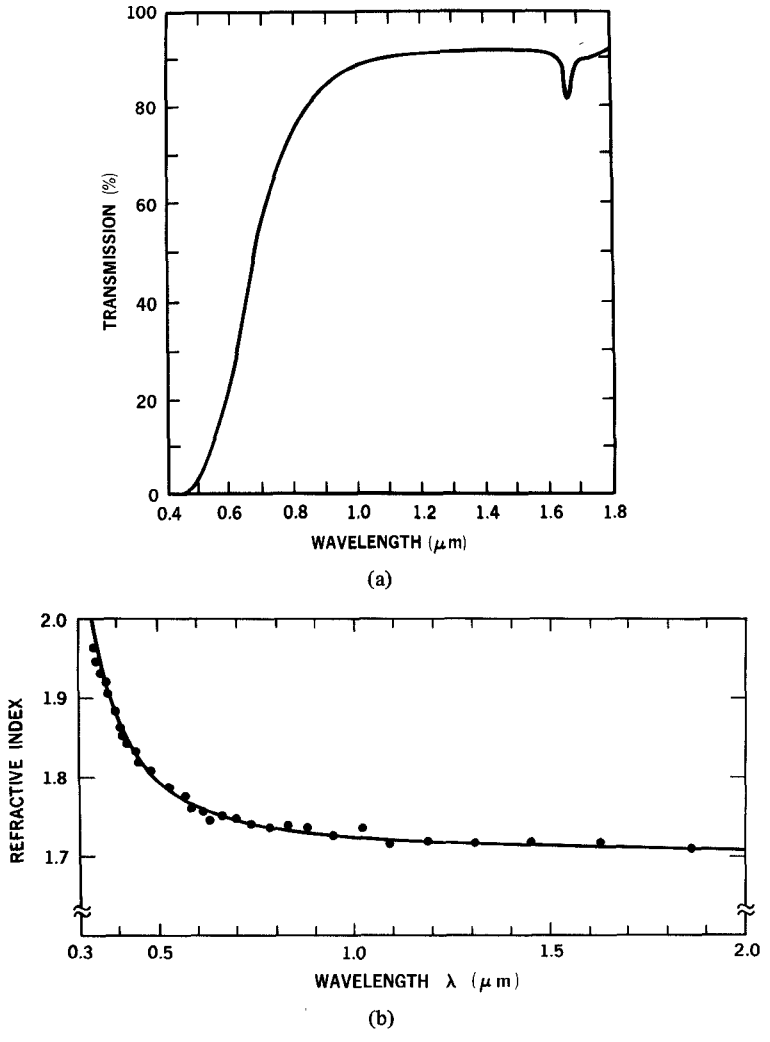

Fig. 2. Optical characteristics of polyimide (P.I.2555). (a) Spectral transmission. (b) Spectral refractive index.

In addition to having a large index and low loss, polyimide is easily etched using either an oxygen plasma or alkaline etchants. Since partially cured polyimide is solvable in basic solutions, the film could be patterned using AZ1350J resist, and then etched using the same AZ303 developer used to process the resist. After full curing, the film becomes chemically resistant. The use of an adhesion promoter [34] was necessary to ensure good adhesion of the polyimide film on the deposited silicon oxide layer; no peeling occurred, even after heating up to 500°C.

IV. Design for DSWI Structure

In what follows, design parameters for the passive waveguide are discussed with respect to the radiation loss due to the higher index substrate, mode-profile matching at the joint, and tolerances in fabrication. Control of reflectivity at the facet is also discussed.

A. Cladding Layer Thickness

Radiation power losses L of a fundamental TE mode in the active and passive waveguides due to the higher index substrate and the cap layer in the case of the active waveguide is given by the following formula [31]:

$$L_i\,(\text{dB/unit length}) \simeq 35\frac{\kappa_i^2\{k_0^2(n_{i1}^2-n_{i2}^2)-\kappa_i^2\}\sqrt{(k_0^2(n_3^2-n_{i2}^2)-\kappa_i^2)}}{k_0^5 n_{i1}(n_3^2-n_{i2}^2)(n_{i1}^2-n_{i2}^2)(1+\kappa_i b_i)}e^{-2\kappa_i d_i} \quad (i=a \text{ or } p) \quad (1)$$

where $k_0 = 2\pi/\lambda$, λ is the wavelength, n_{i1} and n_{i2} $(i = a \text{ or } p)$ are refractive indexes of the core and the cladding layers of the active or the passive waveguide, respectively, n_3 is the refractive index of the higher index substrate or stop-etch layer in Fig. 1(a), $2b_i$ and d_i $(i = a \text{ or } p)$ are the thicknesses of the core and the cladding layer of the active or the passive waveguide, respectively, and $\kappa_i (i = a \text{ or } p)$ is the transverse decay constant of the field given by

$$\kappa_i = \sqrt{k_0^2(n_{i1}^2-n_{i2}^2)-\gamma_i^2} \quad (2)$$

where γ_i is a root of the following equation:

$$\gamma_i b_i = \tan^{-1}\left[\frac{\sqrt{k_0^2(n_{i1}^2-n_{i2}^2)-\gamma_i^2}}{\gamma_i}\right]. \quad (3)$$

Results of calculations for the InGaAsP/InP heterostructure active waveguide and the polyimide/SiO_x $(x \sim 2)$ passive waveguide, previously discussed in Section III, are shown in Fig. 3.

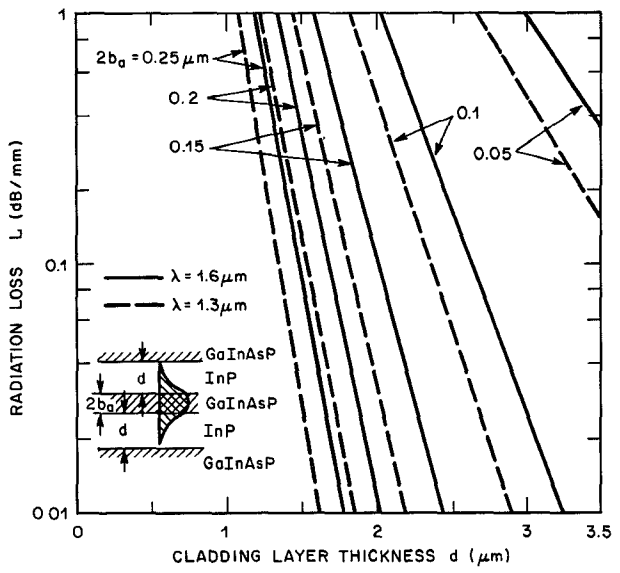

(a)

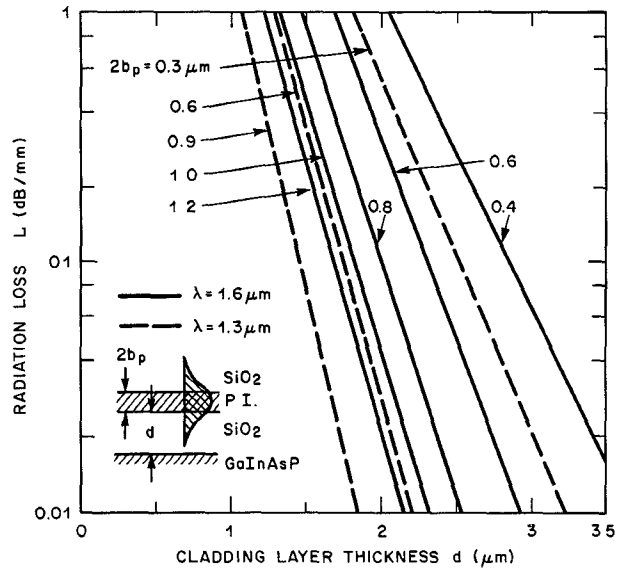

(b)

Fig. 3. Theoretical radiation loss due to higher index substrate. (a) Active waveguide: refractive indexes of 3.56(3.51) and 3.17(3.22) are used for InGaAsP and InP, respectively, for a wavelength of 1.6(1.3) μm [36]. (b) Passive waveguide: refractive indexes of 1.72 and 1.55 are used for polyimide and silicon oxide layer.

As an example of a design of waveguide parameters, if we choose values of the active layer thickness, the passive core, and cladding layer thicknesses as 0.15, 0.8(0.6), and 2 μm, respectively, the radiation loss is less than 0.1 dB/mm for a wavelength of 1.6(1.3) μm.

B. Mode-Profile Matching

In order to suppress scattering loss at the butt joint between the active and the passive waveguides, mode profiles in both waveguides should be matched. An ideal mode-profile matching is obtained under the following conditions:

$$\sqrt{n_{a1}^2 - n_{a2}^2} = \sqrt{n_{p1}^2 - n_{p2}^2} \quad \text{and}$$

$$b_a = b_p. \tag{4}$$

In the case of a nonideal condition, which is more practical, the degree of mode-profile matching is evaluated by the following mode-profile matching factor:

$$\eta = \frac{\left\{\int E_a(y)E_p(y)\,dy\right\}^2}{\int E_a^2(y)\,dy \int E_p^2(y)\,dy} \tag{5}$$

where $E_i(y)\,(i = a \text{ or } p)$ is an electric field distribution in the active or the passive waveguide as given by

$$E_i(y) = \begin{cases} \cos \gamma_i y & \cdots |y| \leqslant b_i \\ \cos \gamma_i b_i e^{-\kappa_i(|y|-b_i)} & \cdots |y| > b_i \end{cases} \tag{6}$$

where γ_i and $\kappa_i (i = a \text{ or } p)$ are given by (2) and (3). In the case that the core thickness of the active waveguide is smaller than that of the passive waveguide, (5) is represented as follows:

$$\begin{aligned} \eta = \Bigg[& \frac{\sin(\gamma_a + \gamma_p)b_a}{\gamma_a + \gamma_p} + \frac{\sin(\gamma_a - \gamma_p)b_a}{\gamma_a - \gamma_p} \\ & + 2\,\frac{1}{\kappa_a}\,\frac{1}{1 + \left(\dfrac{\gamma_p}{\kappa_a}\right)^2} \cos \gamma_a b_a \\ & \times \left\{ \cos \gamma_p b_a - \frac{\gamma_p}{\kappa_a} \sin \gamma_p b_a \right. \\ & \left. - e^{-\kappa_a(b_p - b_a)} \left(\cos \gamma_p b_p - \frac{\gamma_p}{\kappa_a} \sin \gamma_p b_p \right) \right\} \\ & + 2 \cos \gamma_a b_a \cos \gamma_p b_p \frac{e^{-\kappa_a(b_p - b_a)}}{\kappa_a + \kappa_p} \Bigg]^2 \Bigg/ (P_a P_b) \end{aligned} \tag{7}$$

where

$$P_i = b_i + \frac{1}{2\gamma_i} \sin 2\gamma_i b_i + \frac{1}{\kappa_i} \cos^2 \gamma_i b_i \qquad (i = a \text{ or } p). \tag{8}$$

Results of the calculation of (7) are shown for the butt joint between the InP/GaInAsP/InP and SiO_x/polyimide/SiO_x($x \sim 2$) waveguides in Fig. 4. For an active core thickness of 0.15 μm, mode-profile matching of 96 percent can be obtained by choosing passive core thickness of 0.7 or 0.6 μm for wavelengths of 1.6 or 1.3 μm, respectively. The tolerance in adjusting the passive core thickness is as wide as ±50 percent for 90 percent mode-profile matching.

C. Reflectivity Control at Facet

By coating the facet with a dielectric film, the reflectivity at the facet between the active and the passive waveguide can be adjusted. Suppression of the reflection can be attained by anti-reflecting coating with a material of index n_{AR} and thickness t_{AR} which are given by the following well-known formula:

$$n_{AR} = \sqrt{n_a^* n_p^*}$$

$$t_{AR} = \frac{\lambda}{4 n_{AR}} \tag{9}$$

where $n_i^* (i = a \text{ or } p)$ is an equivalent index given as follows:

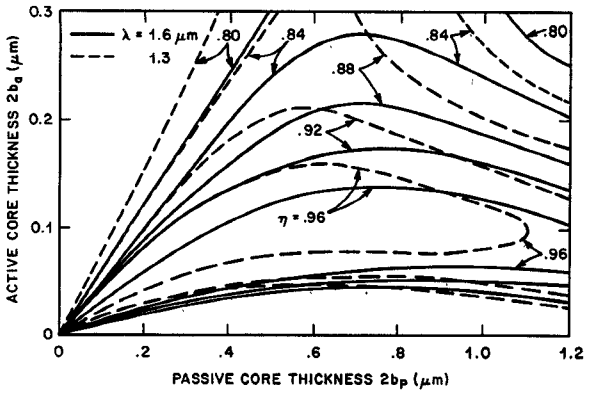

Fig. 4. Theoretical mode-profile matching: same data for index are used as Fig. 3.

$$n_i^* = \sqrt{n_{i1}^2 - (\gamma_i/k_0)^2}. \tag{10}$$

For antireflection at the interface between the InP/GaInAsP/InP and SiO_x/polyimide/SiO_x($x \simeq 2$) waveguides, a TiO_2 evaporation coating of 1600 Å (1300 Å) is applicable for a wavelength of 1.6(1.3) μm.

On the other hand, by coating a single layer of low-index material a quarter wavelength thick, for example, MgF_2(n = 1.35), refelectivity can be increased up to 30 percent for the InP/GaInAsP/InP and SiO_x/polyimide/SiO_x interface. Multilayer dielectric coating can further tailor reflectivity.

D. Tolerance in Fabrication

An offset between the centers of the active and the passive waveguide causes mode-profile mismatching and, therefore, scattering loss. Tolerances in the offset, i.e., deposition thickness of the lower cladding layer, and in the adjustment of the core thickness, i.e., the spin-coating thickness, is examined by calculating the mode-profile matching factor (5), introducing the offset x as follows:

$$\eta(x) = \frac{\left\{\int E_a(y-x)E_p(y)\,dy\right\}^2}{\int E_a^2(y)\,dy \int E_p^2(y)\,dy}. \tag{11}$$

Results of the calculation for the InP/GaInAsP/InP and SiO_x/polyimide/SiO_x waveguide joint are shown in Fig. 5. The power coupling efficiency remains greater than 80 percent for a deposition thickness within ±0.2 μm or ±10 percent and a spin coating thickness ±0.3 μm or ±50 percent in our material combination. The above-mentioned precisions are easily attained due to the low rate deposition and a controlled spin coating.

V. Experimental Demonstration of DSWI

We fabricated an integrated laser waveguide as shown in Fig. 6 using the above-mentioned process and material combination. GaInAsP/InP heterostructure wafers were grown by liquid phase epitaxy on (100) InP substrates in the following sequence: an n-InP buffer layer, an n-GaInAsP stop-etch layer of 0.3 μm, an n-InP cladding layer of 2.2 μm, an undoped GaInAsP active layer (λ_g = 1.3 μm) of 0.15 μm, a p-InP cladding layer of 1.5

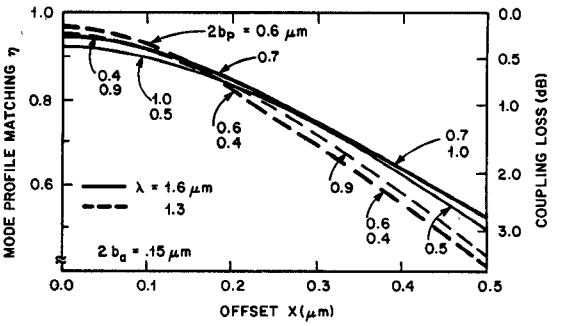

Fig. 5. Theoretical coupling efficiency between GaInAsP/InP and polyimide/SiO_x waveguides.

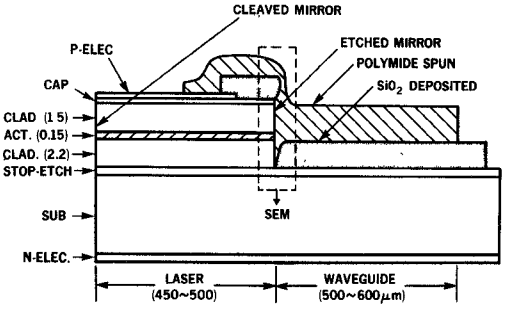

Fig. 6. Structure of integrated laser-waveguide device.

μm, and a p^+-GaInAsP cap layer. The typical threshold current density for lasers fabricated from this wafer was 2.2 kA/cm^2 for a cavity length of 330 μm.

Wafers were etched at room temperature using Si_3N_4 masks in the following sequence [29]: etching through the cap layer by the mixture of concentrated HCl and concentrated HNO_3 for 15 s, etching the upper cladding layer by concentrated HCl for 20 s, etching through the active layer by the mixture of concentrated HCl and concentrated HNO_3 for 10 s, material selective GaInAsP active layer etching, and etching the lower cladding layer by concentrated HCl for 60 s. The etching condition of each step was optimized prior to true etching using test pieces, since the etching characteristics were slightly different from wafer to wafer due to slight differences in dopant concentrations and/or stresses at the heterojunctions. However, the quality of the exposed surface was quite homogeneous over the wafer; more than 80 percent of the laser devices from a single wafer with etched mirrors created by the above-mentioned process oscillated at the threshold current density less than 2.0 kA/cm^2 for a cavity length of 300 μm in an independent experiment for evaluation of etched facets [29].

Using the above-mentioned etching process, the (01$\bar{1}$) facet perpendicular to the active layer and the (100) surface of the stop-etch layer were exposed. The (01$\bar{1}$) facet acts as a laser mirror and the (100) surface is used as the substrate for the passive waveguide. Positive and negative contacts were formed by electroplating Au/Zn and Au/Sn, respectively.

For the lower cladding layer, 2 μm of SiO_x was deposited at a rate of 0.03 μm/min by thermal evaporation of SiO in an oxygen ambient as shown in Fig. 7. Contact windows were opened by liftoff using thick photoresists. For the core layer, polyimide was spun at 6000 revolutions/min and then baked

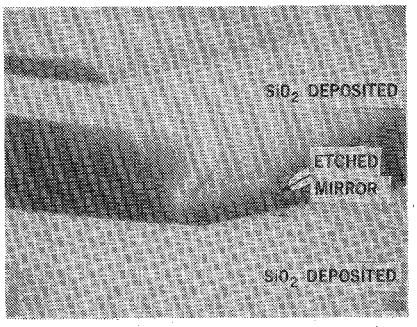

Fig. 7. SEM view after SiO_x deposition.

at 130°C for 5 min. After opening the contact window by photolithographic patterning, polyimide was fully cured at 200°C for 2 h. The thickness of the polyimide layer was 2 μm. A cross-sectional view at a butt-joint interface is shown in Fig. 8. After cleaving, devices were soldered on brass blocks and gold wires were soldered on the p-side electrode.

Typical threshold current density of the laser-waveguide device was 2.0 kA/cm^2 for a cavity length of 430 μm, in spite of the reduction in Fresnel reflectivity down to 0.12 at the etched facet due to the waveguide connection.

Fig. 9(a) and (b) shows top views of the device on the IR-TV screen: the laser was operated at $I = 1.8\ I_{th}$ and a duty ratio of 10^{-3}. The light generated in the etched-facet laser coupled into the passive waveguide (multimode in this case), propagated along the waveguide, and came out the end of the waveguide as shown in Fig. 9(c).

The coupling efficiency between the laser and the waveguide was estimated as follows (Fig. 10). The output powers were measured from the waveguide end and the cleaved facet which was coated with the polyimide to equalize the reflectivity to that of the etched facet butt-jointed with the waveguide. The output power C from the cleaved facet and the output power W from the waveguide end were plotted versus current density as shown in Fig. 10 where the configuration used for the measurement is also shown. From the ratio W/C of the power from the waveguide end to that from the cleaved facet, taking the reflection of 10 percent at the waveguide end into account, the total efficiency of the coupling and the waveguide transmission was estimated as 81 percent. The curve designated by S in Fig. 10 corresponds to the sum of the power scattered upward from the joint and the power spontaneously radiated. The power scattered upward from the joint was 5 percent of the output power C. The scattering loss at the joint can be reduced furthermore by optimizing waveguide parameters. From the earlier loss measurements [Fig. 2(a)], we estimate that the actual butt-joint coupling efficiency is only slightly higher than this.

VI. Conclusion

The deposit/spin waveguide interconnection is proposed as a simple and efficient interconnection technique for semiconductor integrated optics. Detailed data were given for the waveguide design. A demonstration of laser and polyimide/$SiO_x(x \sim 2)$ waveguide integration by DSWI indicates a promising material combination and the feasibility of the etching technique. A deposit/spin waveguide could also be

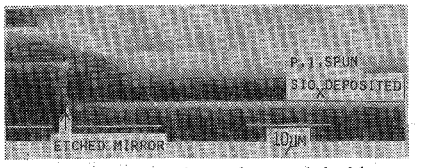

Fig. 8. SEM view of cross section after polyimide coating: marker is 10 μm.

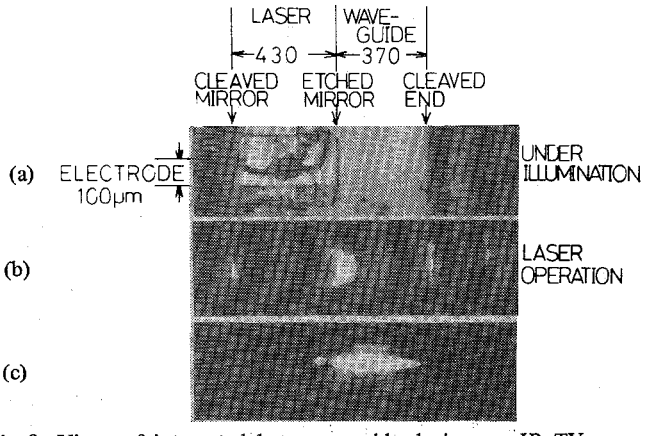

Fig. 9. Views of integrated laser-waveguide devices on IR-TV screen. (a) Top view under illumination. (b) Top view at laser operation. (c) End view of passive waveguide at laser operation.

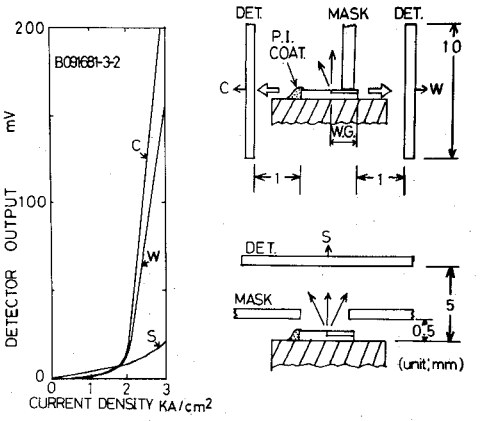

Fig. 10. Estimation of coupling efficiency. From ratio of W/C, more than 81 percent of laser output coupled into waveguide.

useful for other integrated optical devices, such as a distributed Bragg reflector, an optical branching circuit, or an external cavity.

Acknowledgment

The authors would like to acknowledge H. Kogelnik, P. K. Tien, and G. D. Boyd for advice and encouragement; K. Ogawa for advice on paper preparation; A. A. Ballman for the InP substrate; C. A. Burrus, M. R. Biazzo, R. J. Martin, J. A. Rentschler, and L. W. Stulz for advice on fabrication; J. D. McGee for assistance with the LPE system; and R. H. Bosworth for preparing the masks used in this work.

References

[1] J. L. Merz, "Monolithic integration of optical sources and detectors," *Proc. SPIE, Guided-Wave Opt. Surface Acoust. Wave Devices, Syst. Appl.*, vol. 239, pp. 53–60, July 1980.

[2] F. K. Reinhart, "Prospects of monolithic optical integration," *Proc. SPIE, High Speed Detectors*, vol. 272, pp. 66–75, Feb. 1981.
[3] F. K. Reinhart and R. A. Logan, "Monolithically integrated AlGaAs double-heterostructure optical components," *Appl. Phys. Lett.*, vol. 25, pp. 622–624, Nov. 1974.
[4] F. K. Reinhart, R. A. Logan, and C. V. Shank, "GaAs-Al_xGa_{1-x} As injection lasers with distributed Bragg reflectors," *Appl. Phys. Lett.*, vol. 27, pp. 45–48, July 1975.
[5] F. K. Reinhart, R. P. Salathe, R. A. Logan, R. L. Hartman, and L. A. Koszi, "Room temperature CW-operation of taper coupled lasers consisting two-dimensional passive waveguides for monolithic integration," presented at the Topical Meet., Integrated and Guided-Wave Opt., Salt Lake City, UT, 1978, paper PD3.
[6] F. K. Reinhart and R. A. Logan, "Electro-optic frequency and polarization-modulated injection laser," *Appl. Phys. Lett.*, vol. 36, pp. 954–957, June 1980.
[7] S. Wang, "Principles of distributed feedback and distributed Bragg-reflector lasers," *IEEE J. Quantum Electron.*, vol. QE-10, pp. 413–427, Apr. 1974.
[8] Y. Abe, K. Kishino, Y. Suematsu, and S. Arai, "GaInAsP/InP integrated laser with butt-jointed built-in distributed Bragg-reflection waveguide," *Electron. Lett.*, vol. 17, pp. 945–946, Dec. 1981.
[9] Y. Suematsu, M. Yamada, and K. Hayashi, "A multi-hetero-AlGaAs laser with integrated twin guide," *Proc. IEEE*, vol. 63, p. 208, Jan. 1975.
[10] K. Kishino, Y. Suematsu, K. Utaka, and H. Kawanishi, "Monolithic integration of laser and amplifier or detector by twin-guide structure," *Japan. J. Appl. Phys.*, vol. 17, pp. 589–590, Mar. 1978.
[11] K. Utaka, Y. Suematsu, K. Kobayashi, and H. Kawanishi, "GaInAsP/InP integrated twin-guide lasers with first-order distributed Bragg reflectors at 1.3 μm wavelength," *Japan. J. Appl. Phys.*, vol. 19, pp. L137–L140, Mar. 1980.
[12] C. E. Hurwitz, A. J. Rossi, J. J. Hsieh, and C. M. Wolfe, "Integrated GaAs-AlGaAs double-heterostructure lasers," *Appl. Phys. Lett.*, vol. 27, pp. 241–243, Aug. 1975.
[13] K. Aiki, M. Nakamura, and J. Umeda, "Frequency multiplexing light source with monolithically integrated distributed feedback diode lasers," *Appl. Phys. Lett.*, vol. 29, pp. 506–508, Oct. 1976.
[14] C. J. Campbell and D. W. Bellavance, "Monolithic laser/waveguide coupling by evanescent fields," *IEEE J. Quantum Electron.*, vol. QE-13, pp. 253–255, Apr. 1977.
[15] J. L. Merz and R. A. Logan, "Integrated $GaAsAl_xGa_{1-x}As$ injection lasers and detectors with etched reflectors," *Appl. Phys. Lett.*, vol. 30, pp. 530–533, May 1977.
[16] H. Namizaki, M. K. Shams, and S. Wang, "Large-optical-cavity GaAs-(GaAl)As injection laser with low-loss distributed Bragg reflectors," *Appl. Phys. Lett.*, vol. 31, pp. 122–124, July 1977.
[17] P. K. Tien, R. J. Martin, and S. Riva-Sanseverino, "Novel metal-clad optical components and method of isolating high-index substrate for forming integrated optical circuits," *Appl. Phys. Lett.*, vol. 27, pp. 251–253, Aug. 1975.
[18] K. A. James, R. R. August, and J. E. Coker, "Silicon monolithic optical integrated circuits for laser system applications," presented at the Conf. of Laser and Electroopt. Syst., San Diego, CA, May 1976, paper WD11.
[19] J. T. Boyd and C. L. Chen, "Integrated optical silicon photodiode array," *Appl. Opt.*, vol. 15, pp. 1389–1393, June 1976.
[20] G. E. Marx, M. Gottlieb, and G. B. Brandt, "Integrated optical detector array, waveguide, and modulator based on silicon technology," *IEEE J. Solid-State Circuits*, vol. SC-12, pp. 10–13, Feb. 1977.
[21] W. Stutius and W. Streifer, "Silicon nitride films on silicon for optical waveguides," *Appl. Opt.*, vol. 16, pp. 3218–3222, Dec. 1977.
[22] P. K. Tien, R. J. Martin, and G. Smolinsky, "Formation of light-guiding interconnections in an integrated optical circuit by composite tapered-film coupling," *Appl. Opt.*, vol. 12, pp. 1909–1916, Aug. 1973.
[23] T. Kambayashi, C. Kitahara, and K. Iga, "Chemical etching of InP and GaInAsP for fabricating laser diodes and integrated optical circuits," *Japan. J. Appl. Phys.*, vol. 19, pp. 79–85, Jan. 1980.
[24] K. Iga and B. I. Miller, "GaInAsP/InP laser with monolithically integrated monitoring detector," *Electron. Lett.*, vol. 16, pp. 342–343, Apr. 1980.
[25] L. A. Coldren, K. Iga, B. I. Miller, and J. A. Rentschler, "GaInAsP/InP stripe-geometry laser with a reactive-ion-etched facet," *Appl. Phys. Lett.*, vol. 37, pp. 681–683, Oct. 1980.
[26] P. D. Wright, R. J. Nelson, and T. Cella, "InGaAsP double heterostructure lasers ($\lambda = 1.3$ μm) with etched reflectors," *Appl. Phys. Lett.*, vol. 36, pp. 518–520, Apr. 1980.
[27] S. Adachi, H. Kawaguchi, K. Takehei, and Y. Noguchi, "InGaAsP/InP buried-heterostructure lasers ($\lambda = 1.5$ μm) with chemically etched mirrors," *J. Appl. Phys.*, vol. 52, pp. 5843–5845, Sept. 1981.
[28] L. A. Coldren, B. I. Miller, K. Iga, and J. A. Rentschler, "Monolithic two section GaInAsP/InP active-optical-resonator devices formed by reactive-ion-etching," *Appl. Phys. Lett.*, vol. 38, pp. 315–317, Mar. 1981.
[29] K. Furuya, L. A. Coldren, B. I. Miller, and J. A. Rentschler, "Crystallographic facets chemically etched in InGaAsP/InP for integrated optics," *Electron. Lett.*, vol. 17, pp. 582–583, Aug. 1981; and L. A. Coldren, K. Furuya, B. I. Miller, J. A. Rentschler, A. H. Dayem, and P. M. Mankiewich, "Etched mirrors, grooves, and surfaces for GaInAsP/InP integrated optical devices using stop-etch crystal planes," presented at the Topical Meet., Integrated and Guided-Wave Opt., Pacific Grove, CA, Jan. 1982, paper WB1.
[30] F. Furuya, B. I. Miller, L. A. Coldren, and R. E. Howard, "A novel deposit/spin waveguide interconnection (DSWI)–Technique for semiconductor integrated optics," presented at the Topical Meet., Integrated and Guided-Wave Opt., Pacific Grove, CA, Jan. 1982, paper PDP-8.
[31] Y. Suematsu and K. Furuya, "Quasi-guided modes and related radiation losses in optical dielectric waveguides with external higher index surroundings," *IEEE Trans. Microwave Theory Tech.*, vol. MTT-23, pp. 170–175, Jan. 1975.
[32] J. E. Goell, "Rib waveguide for integrated optical circuits," *Appl. Opt.*, vol. 12, pp. 2797–2798, Dec. 1973.
[33] L. I. Meissel and R. Glang, Eds., *Handbook of Thin Film Technology*. New York: McGraw-Hill, 1970, p. 19-9.
[34] PYRALIN P.I.2555 and Adhesion Promoter VM-651, DuPont Co., Wilmington, DE.
[35] For example, K. Mukai, A. Saiki, K. Yamanaka, S. Harada, and S. Shoji, "Planar multilevel interconnection technology employing a polyimide," *IEEE J. Solid-State Circuits*, vol. SC-13, pp. 462–467, Aug. 1978; and L. B. Rothman, "Properties of thin polyimide films," *J. Electrochem. Soc.*, vol. 127, pp. 2216–2220, Oct. 1980.
[36] P. Chandra, L. A. Coldren, and K. E. Strege, "Refractive index data from $Ga_xIn_{1-x}As_yP_{1-y}$ films," *Electron. Lett.*, vol. 17, pp. 6–7, Jan. 1981.

Kazuhito Furuya (M'81), for a photograph and biography, see this issue, p. 1675.

Barry I. Miller, for a photograph and biography, see this issue, p. 1676.

Larry A. Coldren (S'67–M'72–SM'77–F'82), for a photograph and biography, see this issue, p. 1675.

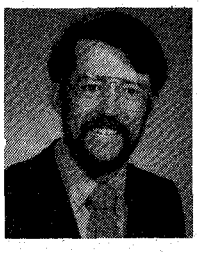

Richard E. Howard (M'81) received the B.S. degree from the California Institute of Technology, Pasadena, in 1970, and the M.S. and Ph.D. degrees from Stanford University, Stanford, CA, in 1972 and 1977, respectively. His major research interest was in the field of superconductivity and superconducting electronics.

He has been a member of the Technical Staff at Bell Laboratories, Holmdel, NJ, since 1978. He is currently interested in the study of novel devices and structures made using new submicron fabrication techniques.

Dr. Howard is a member of the American Physical Society, the American Vacuum Society, and the Materials Research Society.